

## Evolution of two-layer thermohaline systems under surface cooling

By S. I. VOROPAYEV<sup>†</sup> AND H. J. S. FERNANDO<sup>‡</sup>

Environmental Fluid Dynamics Program, Department of Mechanical and Aerospace Engineering,  
Arizona State University, Tempe, AZ 85287-6106, USA

(Received 25 September 1997 and in revised form 13 August 1998)

This paper presents the results of a series of laboratory experiments aimed at understanding the processes associated with surface freezing of a two-layer fluid. The flow configuration consists of a layer of cold, salty water overlying a relatively deep bottom layer of warm, saltier water. This situation is common in high-latitude oceans during periods of rapid ice formation. The experiments were conducted in a tank with well-insulated side and bottom walls, placed in a walk-in freezer with air temperatures from  $-12$  to  $-20^{\circ}\text{C}$ . A system of thermocouples was used to measure the temperatures at fixed levels in water, ice and air. Microscale conductivity and temperature probes were used to obtain vertical profiles of temperature and salinity in the water. In general, when external fluxes of heat and salt are absent, such a system enhances static stability, in the sense that the net density difference between the layers increases with time. When external fluxes of heat (because of surface cooling) and salt (rejected during ice formation) are applied, however, this fluid system may become unstable and overturning of fluid layers is possible. In addition, heat transport from the warmer bottom layer to the colder upper layer may be important, possibly leading to a reduction in the rate of ice formation compared to that of a homogeneous fluid with temperature and salinity identical to the upper layer. Descriptions of such physical processes are given using laboratory experiments, and quantitative measurements of salient parameters are compared with the predictions of a theoretical model developed to explicate the flow evolution.

---

### 1. Introduction

The formation of ice in polar oceans is a topic of considerable scientific and engineering interest, because of its applications to polar oceanography and navigation. On global scales, sea-ice mechanics has a direct bearing on the climate variability through its role in heat and momentum exchange between the atmosphere and oceans and in deep convection of high-latitude oceans. Ice formation in saline water, upon exposure to frigid temperatures, is characterized by the appearance of pure ice crystals at the air–water interface forming an ice sheet; the rejected salt, in part, is trapped within the ice matrix as concentrated brine while the rest is drained out into the underlying fluid. The salinity of ice thus formed is determined by the amount of trapped brine, which in turn depends on such factors as the rate of freezing and the age of the ice. For example, young ice formed from sea water of salinity  $32\text{‰}$  can have a salinity as high as  $25\text{‰}$  (Nakawo & Sinha 1981), but after a few days it decreases

<sup>†</sup> Also at the Institute of Oceanology, Russian Academy of Sciences, Moscow, 117851, Russia.

<sup>‡</sup> Author to whom correspondence should be addressed: e-mail JFernando@asu.edu.

to 8–12‰. Thenceforward, the salinity changes are slow-paced, reaching a value of  $\sim 4$ ‰ after about a year. The brine drainage imposes a destabilizing buoyancy flux on the underlying fluid layer, thus initiating (typically turbulent) convection beneath freezing ice. Under certain conditions, double-diffusive convection is also possible at the ice–water interface (Atkinson & Wake 1988), but it is usually overshadowed by stronger, brine-driven convection (Farhadieh & Tankin 1972; Wakatsuchi & Ono 1983).

The formation and evolution of sea-ice is drastically affected by the temperature ( $T$ ), salinity ( $S$ ) and the density distribution of the underlying water layer (concurrent with oceanographic literature, henceforth, ice formed during the freezing of saline water will be called sea-ice). When  $S > 24.7$ ‰, the density of salt water increases with decreasing  $T$ , with the maximum density occurring at the freezing point  $T_f$ ; this should be contrasted with the  $S < 24.7$ ‰ case where the temperature for maximum density  $T_m$  is higher than  $T_f$ . As a result, in the former case, the entire water column has to be cooled to  $T_f$  before the surface freezing can be initiated. In the latter case, the surface freezing can be initiated soon after the water column reaches  $T_m$ , whereupon liquid subjected to further cooling is retained near the surface, thus dropping its temperature rapidly to  $T_f$ .

Although in typical high-latitude oceans  $S > 30$ ‰ (with the exception of near the boundaries where river run-off can reduce the salinity), the entire depth of the ocean need not be cooled to the freezing point to initiate freezing. This is because of the limit imposed by the stable stratification on the depth of convection. Calculations show that, for typical cooling rates in polar winters, ice formation is not thermodynamically feasible if the depth of the layer being cooled exceeds about 100 m (Zubov 1963). The strongly stratified layer (pycnocline) below the convecting layer also can shield the upper convecting layer from the warm waters below, thus facilitating the maintenance of freezing temperatures in the upper layer.

Zubov (1938) proposed a simple expression for the maximum possible ice thickness  $h_0$  by considering the amount of fresh water contained in the initial stratification:

$$h_0 = \frac{1}{S(\infty)} \int_0^\infty [S(\infty) - S(z)] dz, \quad (1a)$$

where  $z$  is measured vertically downward with  $z = 0$  being the air–water interface. For a two-layer fluid with an upper layer of salinity  $S_1$  and depth  $H_1$  and a lower layer of salinity of  $S_2$  ( $> S_1$ ), (1a) becomes

$$h_0 = H_1(1 - S_1/S_2). \quad (1b)$$

Typical salinity profiles (see e.g. Walin 1993) show that  $S_2 - S_1 \approx 3$ ‰ for the Arctic and  $S_2 - S_1 \approx 0.5$ ‰ for the Antarctic. Estimates based on (1a) and typical profiles give  $h_0 = 5$ –25 m for the Arctic and  $h_0 = 0.5$ –5 m for the Antarctic (Walin 1993). These estimates qualitatively explain why the perennial ice cover in the Arctic (thickness  $\sim 3$ –5 m; see Coachman & Aagaard 1974 and Aagaard, Coachman & Carmack 1981) is much thicker than the winter ice cover of Antarctic (thickness  $\sim 0.5$ –0.75 m; Ackley, Clarke & Smith 1982), despite the extremely cold winters of the latter. It should be noted that the above estimates represent only an upper bound, and do not account for the drastic influence the thermal structure has on the thickness of ice. For example, if the ocean is stably stratified with respect to salt and unstably stratified with respect to heat, the upward heat flux due to diffusion and/or entrainment of the lower-layer fluid into the upper layer can considerably reduce (or even eliminate) ice formation.

The purpose of this paper is to present the results of a laboratory experiment on

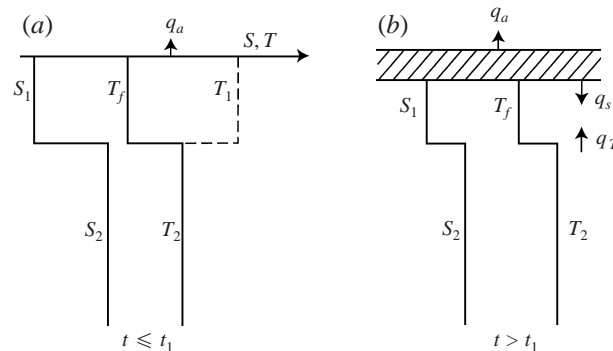


FIGURE 1. A schematic of the distributions of salinity ( $S$ ) and temperature ( $T$ ): (a) initial distribution; (b) distribution when the ice sheet has formed at the surface.

the ice formation in a two-layer fluid. As shown in figure 1(a) the relatively shallow upper layer of depth  $H_1$  contains brackish water of salinity  $S_1$  and temperature  $T_1$ , with  $T_1$  being larger than the freezing temperature  $T_f$ . Initially the bottom layer is saltier ( $S_2 > S_1$ ) and colder ( $T_f < T_2 < T_1$ ), with a depth  $H_2$  ( $> H_1$ ). The pycnocline between the layers is thin, and the ambient air temperature  $T_a$  is below the freezing temperature  $T_f$ . The experiment is of run-down type in that, initially, the thermal convection in the upper layer reduces  $T_1$  to  $T_f$ , whereupon surface ice formation is initiated at time  $t = t_1$ ; continued cooling leads to a new temperature/salinity configuration at  $t > t_1$ , wherein the top layer is maintained near the freezing point  $T_f$  while the bottom layer is still warmer and saltier than the top layer (figure 1b). Now the pycnocline is stable with respect to salt and unstable with respect to heat, thus belonging to the category of 'diffusive interface' of double-diffusive convection (Turner 1979).

At  $t > t_1$ , the system can exhibit three major phenomena: ice formation, brine rejection from growing ice and double-diffusive transport of heat and salt through the density interface. Faster molecular diffusion of heat through the pycnocline, compared to that of salt, may lead to unstable density distributions on either side of the density interface, thus initiating convection in both layers (for example, see Linden & Shirtcliffe 1978). Such double-diffusive transport stabilizes the overall two-fluid system by increasing the density difference between the layers (Turner 1979; Huppert 1971). Conversely, this stabilization is opposed by the ice growth that occurs when the heat flux to ambient air ( $q_a$ ) exceeds the diffusive flux ( $q_T$ ) across the interface. The salt flux ( $q_s$ ) rejected from the growing ice sheet decreases the density jump across the interface by increasing  $S_1$ . If the density jump across the pycnocline is modest, the fluid system can become statically unstable, followed by overturning and mixing during which warm waters from below are convected upward. This upward transport of warmer waters prevents further ice formation or may even lead to the melting of existing ice, if the lower layer has a sufficiently large volume (Welander & Bauer 1977). As pointed out by Martinson (1991) and Walin (1993), however, such overturning is not a necessary condition for hampering the ice growth; diffusive heat flux  $q_T$  and entrainment of warm water from below is sufficient to cause a reduction in the ice growth rate or even the high-frequency oscillatory behaviour that involves switching between partial freezing and melting (called the 'freeze melting' phenomenon). The flow configuration shown in figure 1(b) (corresponding to  $t > t_1$ )

is of interest in this paper, because of its richness in flow phenomena and possible direct applications to geophysical situations described below.

A common feature of both Arctic and Antarctic oceans is the presence of a well-defined pycnocline separating the upper surface waters from underlying warmer saltier waters. In the Arctic, the surface layer is about 25–50 m deep, has a relatively low salinity (28–33.5‰) and has a temperature close to the freezing point (–1.5 to –1.8 °C). Beneath the surface layer, to depths ~100 m, is a layer of subsurface water, mainly controlled by lateral advective processes. In the Eurasian basin of the Arctic, this subsurface layer is isothermal, but a strong variation in salinity (a halocline) can be observed through it. Since the density of water at near freezing temperatures is determined by the salinity alone, this halocline coincides with the Arctic pycnocline; below ~100 m, the temperature increases markedly, but the salinity increases only a little. Subsurface waters in the Canadian basin of the Arctic also show a halocline from 25 m to 100 m, but its temperature has a maximum at ~50–100 m and a minimum at ~150 m, below which the temperature rapidly increases to the deeper Arctic values. On the other hand, the  $T$ – $S$  characteristics of southern oceans are much different. For example, the Weddell sea region is characterized by a deep surface mixed layer of depth ~100 m, underlain by a pycnocline ~20–40 m thick and a nearly homogeneous warm, saltier deep water layer of about 5 km deep (Huber, Mele & Gordon 1989). The temperature below the pycnocline is at ~1 °C in the Weddell warm water regime and < 0.4 °C in the cold regime, with a 2–5 °C temperature difference between the upper and lower layers. The horizontal property gradients are small, and hence processes in the Weddell sea can be represented by a one-dimensional model (Martinson 1991). It is clear that the flow configuration considered in the present study has close similarities to this case, and hence can be a useful model for the winter convection in Weddell sea.

In §2 of the paper, a detailed account of the experimental procedure is given, including problems associated with low-temperature ice-freezing experiments. Section 3 is devoted to presenting qualitative and quantitative observations. To our knowledge, there are no previously reported experiments on the flow configuration considered here, and hence the results are expected to provide useful insights into such fluid systems. As the number of independent parameters involved in the problems is too voluminous to be conveniently handled by conventional dimensional analysis, a general theoretical model is presented in §4 to delineate important governing parameters and to predict the flow evolution. The model is then simplified using reasonable assumptions to predict the system evolution analytically, the results of which will be compared with the experiments. The concluding remarks of the paper are given in §5.

## **2. Experimental installation and method**

The experiments were conducted in a walk-in freezer ( $200 \times 200 \times 200 \text{ cm}^3$ ). During each experiment the temperature in the freezer was held constant and was maintained with an accuracy of  $\pm 1$  °C. In the first set of experiments, homogeneous salt water was used and the second set was carried out with a two-layer stratified fluid. The apparatus consisted of a rectangular tank of cross-section  $31 \times 61 \text{ cm}^2$  and 60 cm deep made of (1.95 cm) thick Plexiglas (figure 2). In some runs, a horizontal grid made of Plexiglas rods of square cross-section ( $1 \times 1 \text{ cm}^2$ ) and a mesh size  $M = 4.5 \text{ cm}$  was used to mix the water. The grid was oscillated in the vertical direction with frequency  $f = 2 \text{ Hz}$  and stroke  $\varepsilon = 2 \text{ cm}$ , with a mean distance of 10 cm from the bottom.

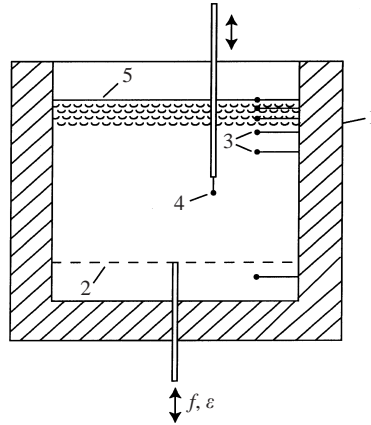


FIGURE 2. A sketch of the experimental apparatus: 1, tank and insulation; 2, oscillating grid (frequency  $f$  and stroke  $\varepsilon$ ); 3, thermocouples; 4, temperature/conductivity probe; 5, growing ice sheet.

To reduce heat losses through the sides and the bottom, sheets of Styrofoam were used as an insulator. A standard method was used to estimate the rate of heat exchange through the surfaces of the tank accurately. In this method, the tank was filled to the top (water depth  $H = 60$  cm) with salt water of salinity 35‰ and temperature  $T_0$  higher than the mean air temperature ( $T_a$ ) in the freezer ( $T_a = -20^\circ\text{C}$ ). The upper surface of the tank was covered with a sheet of Plexiglas, above which a layer of insulation was placed. The water in the tank was mixed periodically by oscillating the grid, and the mean temperature ( $T$ ) of water in the tank was measured as a function of time. The measurements of the non-dimensional temperature excess  $\theta = (T - T_a)/(T_0 - T_a)$  as a function of time ( $t$ ) were plotted, as shown in the log-linear plot of figure 3 (the techniques used for temperature measurements will be discussed later). The solid line through the data points represents the approximation function

$$\theta = (T - T_a)/(T_0 - T_a) = \exp(-t/\tau), \quad (2)$$

with  $\tau = 7100$  min. The heat balance for the water in the tank can be written as

$$\rho c V dT/dt = qB, \quad (3)$$

where  $T(t)$  is the mean temperature given in (2),  $\rho$  and  $c$  are the density and specific heat of water, respectively,  $V = HDL$  is the volume of the tank,  $D$  and  $L$  are the width and length of the tank, respectively, and  $B = 2(HD + HL + DL)$  is the total surface area of the tank. Using (2) and (3), it is possible to obtain an estimate for the mean heat flux ( $q$ ) to ambient air through the surfaces of the tank as

$$q = (T - T_a)\rho c V/B\tau. \quad (4)$$

Using (4), the equivalent heat flux  $q_{0T}$  through the bottom of the tank, which will be used later in §4 to model the heat losses in the system, can be estimated as

$$q_{0T} = q[2H_0(L + D) + LD]/LD, \quad (5)$$

where  $H_0 = H_1 (< H)$  is the total depth of the fluid for experiments with homogeneous water and  $H_0 = H_2$  is the depth of the bottom layer for experiments with a stratified fluid. These two types of experiments will be described below.

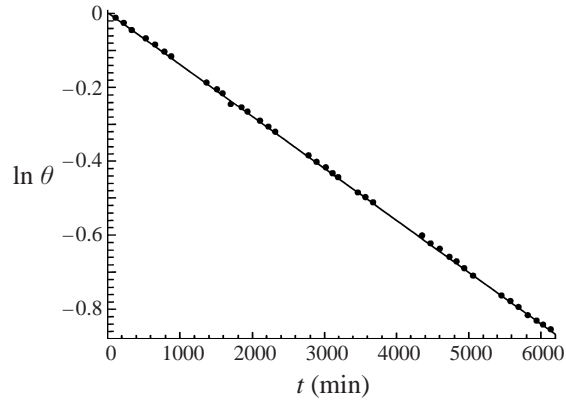


FIGURE 3. Non-dimensional temperature excess ( $\theta$ ) in the tank as a function of time ( $t$ ). A semi-log plot is used; dots show measured values and the solid line shows function (2) with  $\tau = 7100$  min.

The first series of surface-freezing experiments was conducted with homogeneous salt water, and the initial conditions were set up as follows. The tank was filled with salt water of  $S_1 = 32\text{‰}$  to a depth of  $H_1 = 50$  cm. The temperature  $T_1$  of the salt water was higher than the freezing temperature ( $T_f$ ) at this salinity, which is given by (Lide 1993),

$$T_f = -aS_1, \quad (6)$$

where  $a = 0.056\text{°C}(\text{‰})^{-1}$ . After adjusting the temperature of the freezer to a level below  $T_f$ , the water in the tank was thoroughly stirred by oscillating the grid and then the upper cover of the tank was removed. Four experiments were conducted with homogeneous salt water. In two runs, the oscillating grid was turned off after the initial stirring; in the other two runs, the grid oscillations continued during the freezing. The typical velocity (r.m.s.) and (integral) length scale of turbulence  $u_t$  and  $l_t$  induced by the grid at the distance  $x$  from the grid are given by

$$u_t = \gamma_1 M^{1/2} f \varepsilon^{3/2} x^{-1}, \quad l_t = \gamma_2 x, \quad (7)$$

where  $M$  is the mesh size,  $f$  is the frequency and  $\varepsilon$  is the stroke of grid oscillations. For the present grid  $\gamma_1 = 0.3$  and  $\gamma_2 = 0.1$  can be estimated following the procedure used by E & Hopfinger (1986); accordingly near the free surface,  $u_t \approx 0.1\text{ cm s}^{-1}$ .

In the experiments conducted with stratified water, the initial conditions were set as follows. The tank was filled with two layers of water. The bottom layer contained salty ( $S_2 = 37\text{‰}$ ) and relatively warm ( $T_2 \approx 7\text{°C}$ ) water of depth  $H_2 = 35$  cm and the upper layer of depth  $H_1 = 15$  cm contained less salty ( $S_1 = 32\text{‰}$ ) water of approximately the same temperature ( $T_1 \approx T_2$ ) as the bottom layer. The depth  $H_1$  and the salinity jump  $\Delta S = S_2 - S_1$  across the density interface were chosen based on the estimate (1) to obtain a realistic value for the thickness of the ice sheet ( $h_0 \approx 2$  cm) before overturning occurs. The grid oscillations in this experiment were used only to produce a relatively sharp initial density jump between the two layers; during the experiments the grid was held stationary.

An array of six thermocouples was used to measure the temperature at different levels in the tank. One thermocouple was installed just under the free surface of the upper layer and the other five were 0.5, 1.5, 3.5, 9 and 45 cm below the free surface. Thermocouples were fixed to a thin Plexiglas supporting rod, which was positioned vertically at a corner of the tank. The thermocouple wires were bent at right-angles to

the rod, overhung a distance  $\approx 10$  cm from the corner of the tank, and aligned parallel to a plan-view diagonal of the tank. The vertical temperature distribution within air just above the free surface was measured using a thermocouple attached to a traversing mechanism. A standard digital thermometer with electronically compensated reference temperature (accuracy  $\pm 0.1^\circ\text{C}$ ) was used to scan the temperature at different levels periodically. During the experiments, water surrounding some of the thermocouples near the surface froze, thus providing an opportunity to measure the temperature distribution within the ice sheet.

Vertical profiles of conductivity and temperature in the stratified experiments were measured periodically using a four-electrode microscale conductivity probe (with spatial resolution  $\pm 0.1$  cm) and a small thermocouple (of time constant  $\leq 0.15$  s). The two probes were located with a fixed separation of 0.1 cm. These probes were mounted onto an end of a glass capillary tube, which in turn was attached to the end of a thin metal rod that was moved vertically by a stepper-motor-driven traverse. In some cases, the probes were held stationary at selected locations so that time traces of temperature also could be recorded. The temperature was measured with an accuracy of  $\pm 0.1^\circ\text{C}$ . The microscale conductivity probe and associated electronics were found to have typical sensitivity of  $\approx 15 \text{ mV}(\text{‰})^{-1}$ , with a noise level  $\leq 0.1$  mV. The conductivity probe, however, had a small drift; hence it was calibrated *in situ* before and after an experiment, based on which appropriate corrections were introduced to the data. Using the measured temperature and conductivity profiles, the salinity profiles were calculated. In these calculations, the following equation that gives conductivity ( $\sigma$ ) as a function of temperature and salinity was used (Popov, Fedorov & Orlov 1979):

$$\sigma = \sigma_0 + A(S - S_0) + B(T - T_0), \quad (8)$$

where  $\sigma_0 = 2.92 \Omega^{-1} \text{ m}^{-1}$ ,  $A = 7.5 \times 10^{-2} \Omega^{-1} \text{ m}^{-1}(\text{‰})^{-1}$ , and  $B = 8.8 \times 10^{-2} \Omega^{-1} \text{ m}^{-1}(\text{°C})^{-1}$  for  $S_0 = 35 \text{ ‰}$  and  $T_0 = 0^\circ\text{C}$ . Because of the small drift associated with the probe at low temperatures, the accuracy of salinity measurements was only moderate ( $\approx 1\%$ ).

Some technical details pertinent to the experiments are noteworthy. First, in between the measurements, the probe must be placed in the bottom layer where the temperature is warmer than the freezing temperature. If the probe remains in the upper layer, where the temperature is at or near the freezing point, small ice crystals may form at the platinum electrodes, leading to erroneous measurements. Secondly, to avoid the freezing of ice onto the probe support, it must be covered with Teflon. Thirdly, a protective device must be installed to avoid damage to the glass tip of the extremely delicate conductivity probe. To this end, a safety ring was installed near the probe tip and all the measurements were made starting approximately 3 cm below the ice sheet. Estimates of possible errors due to such a protective mechanism were made *a priori*, and the errors were found to be negligible. For a four-electrode conductivity microprobe (two electrodes are active and the two are passive), the protective ring is not expected to alter the electric field around the probe tips. The hydrodynamic influence of the ring on the measurements, however, cannot be automatically discounted and hence the protective ring needed to be designed to minimize such an influence. It consisted of a plastic ring of diameter 2 cm (thickness 0.1 cm), installed 0.2 cm ahead of the small probe tip, so that the wake produced by the ring during the motion of the probe lay outside radius of influence of the probe.

During the experiments, the thickness of the ice sheet was measured periodically. For this purpose, small holes were drilled in the ice cover, and the thickness mea-

measurements were read from a side view of the tank using a thin plastic rod with 0.1 cm markers highlighted with fluorescent paint. Typically 3–4 readings were made at different places and the mean value was used as the thickness of the ice sheet. During the course of these measurements, 2–3 ml of water was sucked through these measurement holes to release the pressure in the tank because of some thermal/phase expansion of ice. After each experiment, a block of ice ( $15 \times 15 \text{ cm}^2$ ) was cut from the ice sheet and, after melting, its salinity was determined using a standard temperature-compensated refractometer (accuracy  $\pm 0.5\%$ ). In some cases, cuts made at different levels in the ice block were used to measure the salinity at different levels.

### 3. Observational results

In this section, a qualitative description of the observations is presented, together with some measurements of temperature and salinity. A theoretical model for the problem at hand and comparisons of measurements with the model predictions will be described in the next section. First, consider the case where initially the water is homogeneous in salinity and temperature, with the water temperature near the freezing point. When the upper cover of the tank is removed and cooling is initiated, intense heat convection is developed in the fluid. The surface layer becomes slightly supercooled (Katsaros & Liu 1974), and ice crystals begin to form near the surface. Note that, in contrast to frazil ice that forms inside slightly supercooled turbulent water away from the free surface (Martin 1981; Voropayev Fernando & Mitchell 1995) (also see Foster 1969), the surface ice does not require artificial seeding to trigger its formation. A possible explanation is that, in the latter case, there are enough ice nuclei in the cool air to initiate ice formation at the water surface (Katsaros & Liu 1974), whereas in the former case such nuclei do not penetrate to deeper layers to initiate the formation of frazil ice.

With time, small discoid crystals fuse together forming large platelets, and soon a thin ( $\approx 0.05 \text{ cm}$ ) ice cover appears at the surface. Typical time records of temperature taken during this initial ice formation demonstrate a cyclic variation with a period of about 0.5–1 min; Figure 4 shows a corresponding temperature record taken at a depth of 1 mm under the ice surface; note the regular fluctuations until the water column above the thermocouple is totally frozen at the time indicated by the arrow. As time progresses, more discoid ice crystals are formed under the thin ice cover, fusing together and forming a rigid ice matrix, within which some salt water appears to be trapped. Because the ice crystals are made of pure water, the brine drained from the ice is saltier than the surrounding water and haline convection is possible (Foster 1969; Farhadieh & Tankin 1972).

Typical time records of temperature and salinity/conductivity measured under the growing ice sheet, after the initial period, show periodic pulsations of salinity but not of temperature (figure 5). These positive salinity pulsations are a result of slowly sinking elements of brine rejected from the ice sheet. Typical velocity (r.m.s)  $u_c$  and (integral) length  $l_c$  scales induced by this saline convection can be estimated as

$$u_c = \gamma_3 (g H_1 q_{is} / \rho)^{1/3}, \quad l_c = \gamma_4 H_1, \quad (9)$$

where  $\gamma_3 = 1.3$ ,  $\gamma_4 = 0.25$ ,  $g$  is the gravitational acceleration,  $H_1$  is the water depth,  $\rho$  is the water density and  $q_{is}$  is the (density) flux of salt rejected from the ice (e.g. see Fernando 1989).

The initial rate of ice formation is rather high and it takes less than an hour to form an ice sheet of thickness 0.5–1 cm. A typical ice sheet, as viewed from the



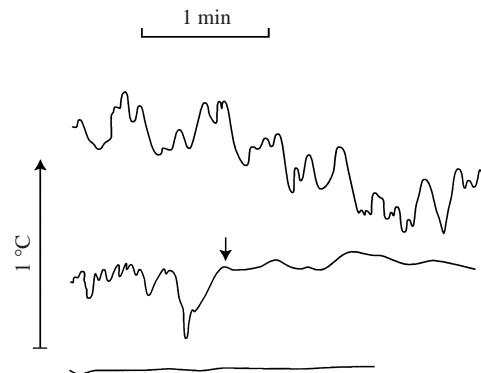


FIGURE 4. A typical continuous time trace of temperature in the upper few millimetres of salt water during the initial growth of ice cover (for convenience, divided into three parts starting at the top and continuing to the bottom).  $S = 32\text{‰}$ ,  $T_a = -19^\circ\text{C}$ , the arrow shows the instance where the surface is completely frozen and the temperature at this moment was  $T_0 = -2.1^\circ\text{C}$ . In this run the grid near the bottom was oscillated with  $f = 2\text{ Hz}$  and  $\varepsilon = 2\text{ cm}$ .

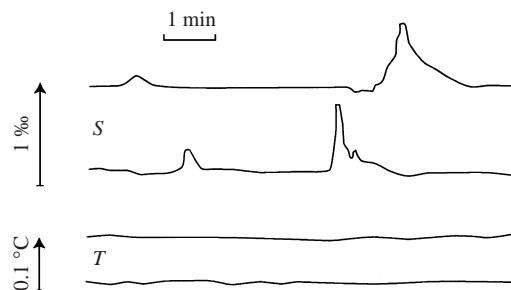


FIGURE 5. Typical time records (divided into two parts) of temperature and salinity (conductivity) measured at a depth of 5 cm below a rapidly growing ice sheet of thickness 2.5 cm. Homogenous salt water with  $S_1 = 32\text{‰}$ , and  $T_a = -19^\circ\text{C}$  was used. The oscillating grid was turned off during the measurements and was then turned on again.

top during this phase, is shown in figure 6(a). A characteristic feature of this ice is relatively large ( $\approx 1\text{--}2\text{ cm}$ ) ice needles. Later these needles form large stellar crystals under the surface (figure 6b). On average, the upper ice surface is smooth and stellar crystals are located mostly at the bottom of the ice cover (also, see figure 9 in Weeks & Ackley 1986). With time, the rate of ice formation decreases because the growing ice sheet reduces the heat flux to the surrounding air. After 5–6 h, the morphology of the upper surface of the ice cover undergoes marked changes, and fine grains appear at the surface (figure 6c). Surface patterns very similar to those shown in figure 6, were observed in all experiments carried out with both calm homogeneous and calm stratified fluids.

In calm water, at large rate of ice formation, the planes of discoid ice crystals growing at the bottom of the ice sheet are mostly oriented vertically (figure 7a). In slightly turbulent water, the orientation is more or less random initially when the rate of ice formation is relatively high (figure 7b); the orientation becomes mostly horizontal when the rate of ice formation decreases (figure 7c). These differences can be explained by considering the relative magnitudes of typical convective ( $u_c$ ) and turbulent ( $u_t$ ) velocities under the ice sheet. In a calm fluid ( $u_t = 0, u_c \neq 0$ ), the preferable direction for convective velocity ( $u_c$ ) just under the ice sheet is vertical,

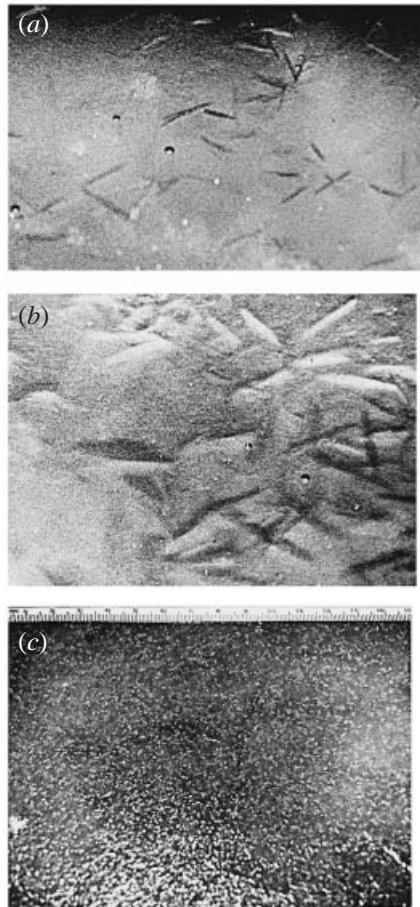


FIGURE 6. Typical structure of a growing ice sheet as viewed from the top. The photographs were taken of approximately the same area at different times ( $t$ ) from the time where the surface was totally frozen (compare the positions of frozen air bubbles in the two first photographs): (a)  $t = 20$  min, (b) 120, (c) 600. The scale is in cm. Slightly turbulent homogenous salt water,  $S = 32\text{‰}$ , was used with  $T_a = -19^\circ\text{C}$ .

and hence most of the discoid ice crystals prefer a vertical orientation. In slightly turbulent water ( $u_t = 0.1\text{ cm s}^{-1}$ ) the velocity field under the ice is dominated by the horizontal velocity that arises due to the imposed turbulent velocity field, and a good estimate of this horizontal velocity is given by (7); see Kit, Strang & Fernando (1997). Conversely, the convective velocity  $u_c$  due to the salt flux is expected to be given by (9); typical values are  $u_c \approx 0.4\text{ cm s}^{-1}$  for high rates of ice formation and  $u_c \lesssim 0.1\text{ cm s}^{-1}$  for low rates. Thus, in slightly turbulent water with  $u_c \approx u_t$ , one may expect chaotic orientation of discoid ice crystal at high rates of ice formation. When the ice formation rate is small, horizontal orientation of ice crystal planes can be expected when  $u_c < u_t$  whereas vertical orientation occurs mostly in calm water when  $u_t = 0$ ,  $u_c \neq 0$ .

It was observed that the ice thickness of experiments with calm water was systematically less (20–25%) than that with slightly turbulent water, conducted at the same air temperature. A possible explanation for this disparity can be advanced as follows.

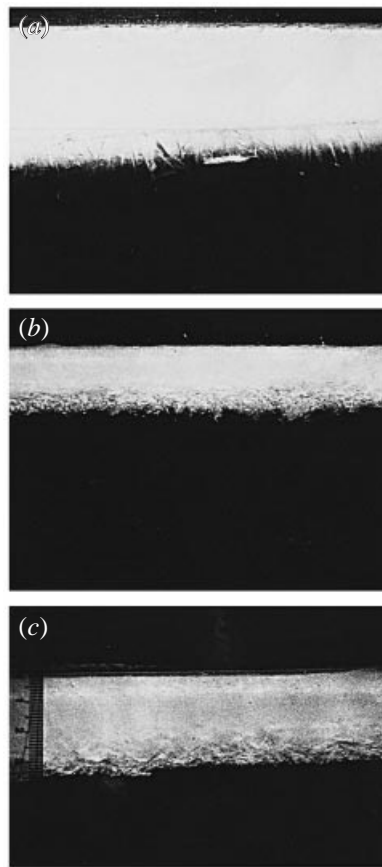


FIGURE 7. A typical view of the growing ice sheet viewed from the side: (a) calm fluid; (b) slightly turbulent fluid with a relatively high rate of ice formation; (c) slightly turbulent fluid at relatively low rate of ice formation. The scale is given in the last photograph. For better lighting and view, the camera was set at an angle to the tank wall and the horizontal ice-water interfaces in (a) and (c) look tilted.

In calm water, some ice crystals are formed and deposited on the side and bottom walls of the tank as well as on the stationary grid (figure 8*a*). A small, but finite heat flux through the tank surfaces (see (5)) may initiate local supercooling and hence such ice deposition is possible (also, see Ettema, Karim & Kennedy 1984; Omsted 1985). As a result, a part of the ice is excluded from the ice sheet at the surface. In slightly turbulent water, when the grid oscillates, such deposition is hardly possible, because of turbulent mixing over the entire depth of the fluid, which prevents the formation of locally supercooled fluid. As a result, the ice forms only at the surface (figure 8*b*). Therefore, there is a possible lack of generality of the results obtained in calm water experiments carried out with homogeneous fluids; henceforth we will only discuss the measurements carried out with slightly turbulent water ( $u_t \neq 0$ ).

Typical vertical profiles of temperature ( $T_i$ ) obtained from within the growing ice sheet at different times are shown in figure 9. Soon after the ice sheet begins to form, an approximately constant temperature gradient is established in the ice sheet. The temperature at the bottom of the ice sheet does not change significantly with time and remains approximately equal to the water temperature, which is at the freezing

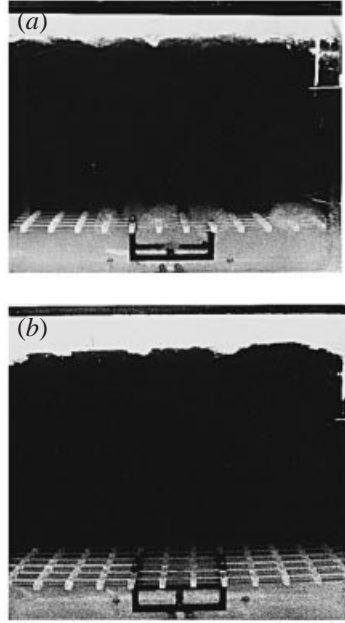


FIGURE 8. The side view of the tank, with the ice sheet at the surface: (a) calm water; (b) slightly turbulent water. Numerous ice crystals are clearly seen in the lower part of the tank and in the vicinity of the stationary grid (a), while the oscillating grid and the lower part of the tank are clear of ice in (b).

point ( $T_f$ ). The temperature at the upper ice surface ( $T_0$ ) decreases gradually with time in such a manner that the mean gradient of temperature within the ice also decreases. Using these data (also, see Nakawo & Sinha 1981), the temperature ( $T_i$ ) in the ice sheet of the thickness  $h$  may be approximated as

$$T_i = T_0 + (T_f - T_0)z/h, \quad (10)$$

where  $z$  is the distance measured downward from the surface. Also, the upward heat flux ( $q_{iT}$ ) through the ice can be estimated as

$$q_{iT} = K_i(T_f - T_0)/h, \quad (11)$$

where  $K_i$  is the thermal conductivity of sea ice ( $K_i = 3.4 \times 10^{-3} \text{ cal cm}^{-1} \text{ s}^{-1} (\text{°C})^{-1}$ ; Weeks & Ackley 1986).

Due to practical difficulties, the salinity distribution in the ice was not measured during the experiments. At the end of each run, however, a block of ice cut from the ice sheet was sliced so that the averaged salinity at various vertical levels of the original ice cover could be measured. No systematic variation with depth was found, and below the salinity ( $S_i$ ) within the ice sheet is considered approximately homogeneous with depth:

$$S_i \approx \text{const.} \quad (12)$$

The average  $S_i$ , obtained from all the runs, was found to be  $16 \pm 2\%$ , a result which is in agreement with the typical values (15–20%) reported for young sea ice (Pounder 1965; Nakawo & Sinha 1981).

A typical vertical profile of the non-dimensional air temperature ( $\theta_a = (T - T_0)/(T_a - T_0)$ ) above the ice surface ( $z = 0$ ) is shown in figure 10. These data were obtained

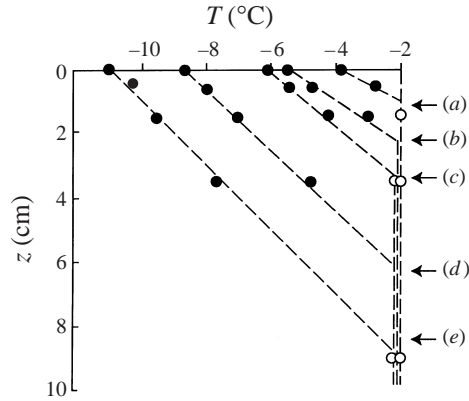


FIGURE 9. Vertical temperature distribution in the growing ice sheet. Symbols are the measured values in ice (●) and in water (○) below the ice sheet; dashed lines represent a linear approximation and arrows show the ice thickness. Times from the beginning of the ice formation are: (a)  $t = 90$  min, (b) 230, (c) 345, (d) 900, (e) 1500. Slightly turbulent homogenous salt water of  $S = 32\%$  was used with  $T_a = -19^\circ\text{C}$ .

by averaging over a period of 3–5 min of temperature–time traces at different heights from the ice surface. This method appeared to be more accurate than the averaging of vertical temperature profiles taken from traversing probes, because of the strong short-period variability of temperature near the ice surface. A near-surface layer with an approximately constant temperature gradient can be clearly seen in the measurements. The thickness ( $\delta$ ) of this layer, determined by a straight-line fit as shown in figure 10, was taken as the typical thickness of the temperature boundary (sub)layer, in which the heat transport occurs predominantly by the molecular diffusion. Because the Prandtl number of air ( $Pr = \nu_a/\kappa_a$ , where  $\nu_a$  and  $\kappa_a$  are the kinematic viscosity and thermal diffusivity of air, respectively) is of the order of unity, one may expect that the thickness of the viscous (momentum) boundary layer over the smooth ice surface ( $= \nu_a/u^*$ , where  $u^*$  is a characteristic friction velocity) is also equal to the temperature sublayer thickness  $\delta$ . The air circulation within the icebox was held constant during the experiments, and hence one may expect that  $u^* \approx \text{const}$  and thus  $\delta \approx \text{const}$ . The average value of  $\delta$ , as measured in all the experiments, was found to be approximately constant and was equal to  $0.15 \pm 0.03$  cm. Using this result, the heat flux ( $q_{aT}$ ) to the ambient air could be estimated as

$$q_{aT} = K_a(T_0 - T_a)/\delta, \quad (13)$$

where  $K_a$  is the thermal conductivity of air ( $K_a = 5.7 \times 10^{-5}$  cal cm $^{-1}$  s $^{-1}$  ( $^\circ\text{C}$ ) $^{-1}$ ).

In the experiments with two-layer stratified fluids, a step-like initial salinity distribution was used. Typical time records of temperature and salinity profiles, based on an experiment conducted at  $T_a = -19^\circ\text{C}$ , are shown in figures 11 and 12. Initially (at time  $t = -240$  min) the temperature was approximately homogeneous in the upper and bottom layers, but with time the temperature in the upper layer decreased rapidly, as a result of intense cooling at the open surface;  $t = 0$  was selected as the time when the ice cover began to appear at the surface. At this time, the bottom saltier layer was approximately  $6^\circ\text{C}$  warmer than the upper layer, and when the crystals of ice first began to form at the surface, the mean temperature of the upper layer was approximately  $-1^\circ\text{C}$ . Only close to the surface, in a layer of depth  $\leq 0.5$  cm, was the water at its freezing point ( $-1.8^\circ\text{C}$ ). Later, when the surface was totally frozen, the

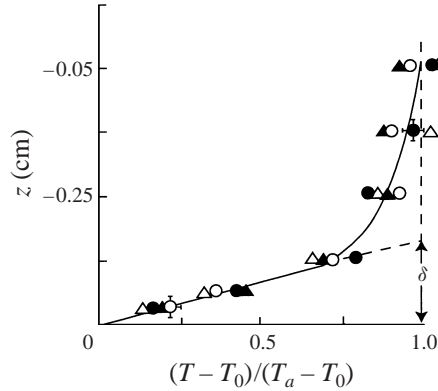


FIGURE 10. The vertical distributions of the non-dimensional air temperature above the ice surface ( $z = 0$ ). The measured values are shown by symbols, and the solid line shows an eye-fitted line. The dashed lines show how  $\delta$  was estimated by extrapolation of a linear fit to the points near the surface. Typical error bars are shown.  $T_a = -12^\circ\text{C}$ :  $T_0 = -3.9^\circ\text{C}$ ,  $h = 2.5$  cm ( $\bullet$ ),  $-5.4, 5.5$  ( $\blacktriangle$ ); and  $T_a = -19^\circ\text{C}$ :  $T_0 = -6.7^\circ\text{C}$ ,  $h = 3.9$  cm ( $\circ$ ),  $-8.4, 6.2$  ( $\triangle$ ).

temperature in the upper layer dropped to near the freezing point, after which its temperatures did not change significantly with time.

Some interesting features can be seen in the data presented in figures 11 and 12. The salinity in the bottom layer practically did not change during the course of the experiment (indicating negligible salt transport through the pycnocline), while salinity in the upper layer gradually increased following the brine rejection during surface freezing. The temperature of the warmer bottom layer slowly decreased with time, mainly because of the heat transport to the colder upper layer (see the estimate below) and partly because of the sidewall heat losses (e.g. see (5)). Note that large differences in molecular heat and salt fluxes through the pycnocline are possible because of the wide disparity of the molecular diffusivities of heat and salt.

The distribution of temperature in the growing ice sheet, as shown in the upper left-hand side of figure 11, is qualitatively similar to the data taken in homogeneous fluids (shown in figure 9), and hence can be approximated by the linear dependence (10) (dashed lines).

The graph presented in figure 13 shows how the air temperature ( $T_a$ ), the ice surface temperature ( $T_0$ ), and the temperatures at different levels ( $T_{0.5}$ ,  $T_{1.5}$ ,  $T_{3.5}$ ,  $T_9$  and  $T_{45}$  – the subscript indicates the depth in cm below the surface) changed with time. Note that the air temperature  $T_a \approx \text{const}$  but both the ice surface temperature and the temperature inside the growing ice sheet gradually decreased with time. The temperature in the middle of the upper water layer ( $T_9$ ) slowly decreased initially and reached the freezing point at  $t \approx 200$  min. Then it remained approximately constant until  $t = 900$  min whence mixing with the bottom layer occurred and  $T_9$  increased by approximately  $1^\circ\text{C}$ . The temperature in the bottom layer ( $T_{45}$ ) also decreased with time at an approximately constant rate ( $dT_{45}/dt \approx 1.0 \times 10^{-4}^\circ\text{C s}^{-1}$ ) until  $t \approx 900$  min. For this cooling rate, the net equivalent heat flux ( $q_\Sigma$ ) through all the horizontal surfaces of the bottom layer could be estimated as

$$q_\Sigma = c\rho H_2 dT_{45}/dt. \quad (14)$$

This gives, for  $H_2 = 35$  cm,  $q_\Sigma = 3.5 \times 10^{-3} \text{ cal cm}^{-2} \text{ s}^{-1}$ , and the heat flux  $q_{1T}$  transported upward from the bottom layer across the density interface can be

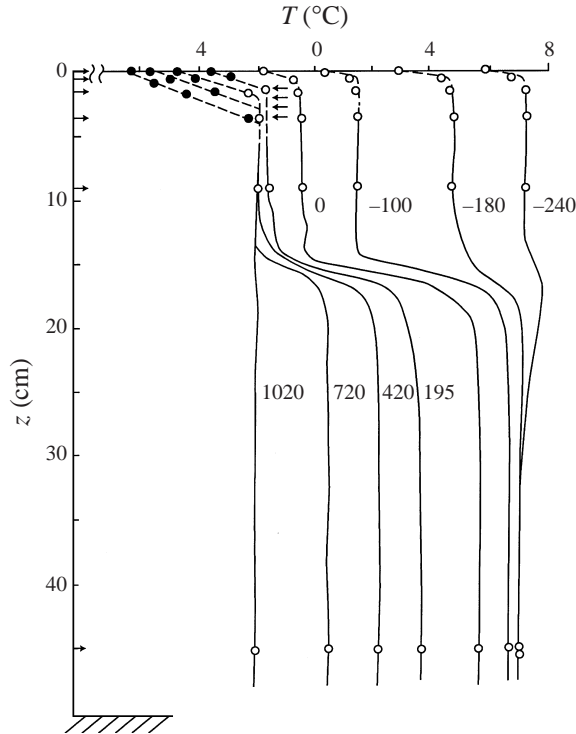


FIGURE 11. A sequence of temperature profiles taken in water layers under the growing ice sheet and within the ice sheet in a two-layer experiment. Numbers show the time ( $t$ ) in minutes measured from the instant where the surface was totally frozen ( $t = 0$ ). Data points represent water (O); and ice (●). Arrows on the  $z$ -axis show the position of thermocouples,  $z = 0; 0.5, 1.5, 3.5, 9$  and  $45$  cm. Arrows next to the profiles at  $t = 195$  show the ice thickness at the different times for  $t > 0$ . For clarity, every second profile is shown. The air temperature  $T_a = -19^\circ\text{C}$ .

estimated as

$$q_{1T} = q_\Sigma - q_{0T}, \quad (15)$$

where  $q_{0T}$  is given by (5).

Following mixing between the layers, the temperature in the system decreased rapidly, reaching the freezing temperature at  $t \approx 1000$  min. The time where the system became neutrally stable (via a series of processes such as salt rejection, diffusion and mixing) can be estimated accurately from the graph shown in figure 14, where the mean differences in salinity ( $\Delta S$ ) and temperature ( $\Delta T$ ) (normalized by initial values  $\Delta S_0$  and  $\Delta T_0$  at  $t = 0$ ) between the layers are shown as functions of time. At the near freezing temperatures, the main contribution to the density comes from salinity, and hence when  $\Delta S \approx 0$  ( $t \approx 900$  min) the density distribution effectively becomes neutral, followed by vertical mixing. The instance where such homogeneity was achieved in the system is indicated by a vertical dashed line in figure 14.

To ensure that significant vertical mixing takes place between the layers, two additional runs were made with qualitative flow visualization. In one run, fluorescent dye was added to the upper layer and in the other to the bottom layer. Visual observations clearly showed that in both cases the dye practically did not penetrate across the pycnocline while it is stable. Only at the end of runs, when  $\Delta S \approx 0$ , did

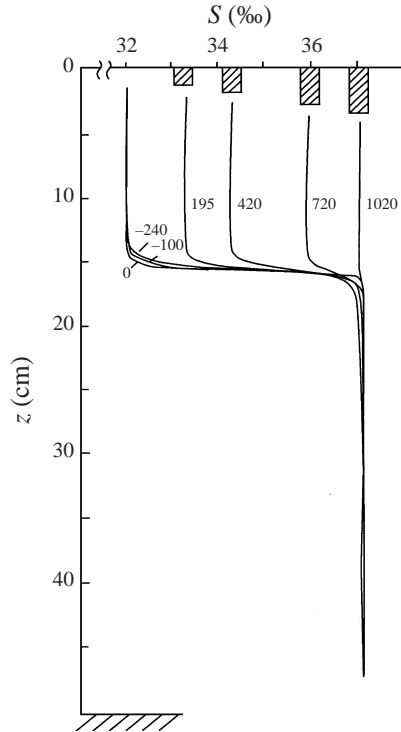


FIGURE 12. Sequence of salinity profiles in water under the growing ice sheet in a two-layer experiment. Numbers show the time ( $t$ ) in minutes from the moment ( $t = 0$ ) the surface is totally frozen. The thickness ( $h$ ) of the ice sheet is shown by the shaded area. For clarity every second profile is shown. The air temperature  $T_a = -19^\circ\text{C}$ .

substantial mixing between the layers occur and the dye distributed in both layers uniformly.

#### 4. Theoretical model and estimates

Based on observations presented in §3 a one-dimensional model for the ice formation in two-layer fluids is developed below. The system under consideration is shown schematically in figure 15. The upper layer of depth  $H_1$  and the bottom layer of depth  $H_2$  contain water of temperature, salinity and density  $T_{1,2}$ ,  $S_{1,2}$ , and  $\rho_{1,2}$ , respectively,  $\Delta T = T_2 - T_1 > 0$ , and  $\Delta S = S_2 - S_1 > 0$ . The temperature interface between these two layers is thicker than the salinity interface and hence the water at the top of the bottom layer is colder than the water below. Thus, gravitational convection develops in the bottom layer, which leads to fluxes of both heat ( $q_{2T}$ ) and salt ( $q_{2S}$ ) across the density interface. The temperature of ambient air ( $T_a$ ) is below the freezing temperature ( $T_f$ ) of the salt water in the upper layer and an ice sheet of thickness  $h$  is formed at the surface of the upper layer.

The density, temperature, and salinity of resulting salt-ice are  $\rho_i$ ,  $T_i$ , and  $S_i$ , respectively. Because the salinity of salt-ice ( $S_i$ ) is less than the salinity of water ( $S_1$ ) in the upper layer, some salt ( $q_{is}$ ) is rejected from the ice sheet into the upper layer during the ice formation. This leads to convection and mixing in the upper layer. In general, the density interface between upper and bottom layers can deepen with a certain (entrainment) velocity, say  $W$ , because the convection in the upper layer is



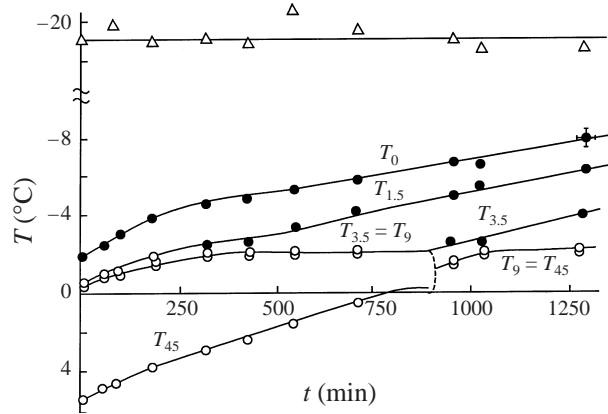


FIGURE 13. A graph showing how the air temperature ( $T_a$ ), ice surface temperature ( $T_0$ ), and the temperatures at different depths ( $T_{0.5}$ ,  $T_{1.5}$ ,  $T_{3.5}$ ,  $T_9$ , and  $T_{45}$ ) below the ice surface change with time. Temperatures in the air and water are shown by open symbols, and solid symbols indicate the readings of the thermocouples which are frozen into the ice. Solid lines show smoothed approximate fits to the experimental data and the dashed line shows the instance where intense mixing occurs. Note that the temperature decreases upward.

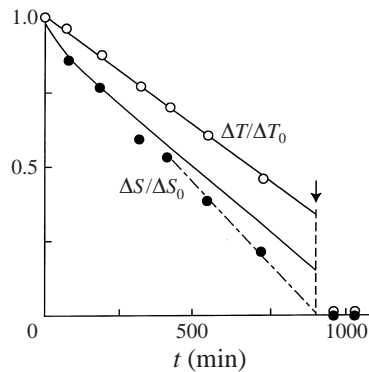


FIGURE 14. Non-dimensional differences of salinity ( $\Delta S/\Delta S_0$ ,  $\bullet$ ) and temperature ( $\Delta T/\Delta T_0$ ,  $\circ$ ) between the two layers as functions of time ( $t$ ). Solid lines show estimates from the model described in §4, the dashed-dotted line shows a linear approximation to the experimental data for salinity and the vertical dashed line and arrow show the time where vertical mixing was initiated.

stronger than that in the bottom layer. The heat losses in the bottom layer through the sidewalls and the bottom of the tank are modelled by an equivalent heat flux ( $q_{0T}$ ) from the bottom. The heat losses in the upper layer through the sidewalls are at least three times less ( $2H_1(L+D)/(2H_2(L+D)) \approx 3$ , see (5)) and hence can be neglected. The heat flux  $q_{1T}$  in (15) is used to model the heat transport from the upper layer to the ice sheet and heat fluxes in the ice sheet ( $q_{iT}$ ) and in the air ( $q_{aT}$ ) above the ice surface are related to each other as

$$q_{iT} = q_{aT}. \quad (16)$$

To derive the governing equations for the problem, consider balances of mass, salinity and heat in the ice sheet (thickness  $h$ ), in the upper layer (thickness  $H_1$ ), and in the bottom layer (thickness  $H_2$ ). Using the notation of figure 15, the mass balances

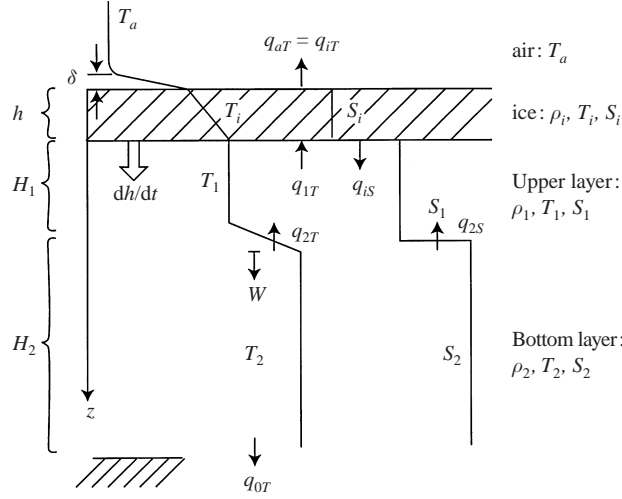


FIGURE 15. A schematic of the system configuration used in developing the model.

of water and ice take the form

$$\frac{d}{dt}(h\rho_i) = \rho_1 \frac{dh}{dt}, \quad (17)$$

$$\frac{d}{dt}(H_1\rho_1) = -\rho_1 \frac{dh}{dt} + \rho_2 W, \quad (18)$$

$$\frac{d}{dt}(H_2\rho_2) = -\rho_2 W. \quad (19)$$

The balances of salt give (here  $S$  must be measured in fractions)

$$\frac{d}{dt}(h\rho_i S_i) = -q_{is} + \rho_1 S_1 \frac{dh}{dt}, \quad (20)$$

$$\frac{d}{dt}(H_1 \rho_1 S_1) = q_{is} + q_{2S} - \rho_1 S_1 \frac{dh}{dt} + \rho_2 S_2 W, \quad (21)$$

$$\frac{d}{dt}(H_2 \rho_2 S_2) = -q_{2S} - \rho_2 S_2 W. \quad (22)$$

The heat balances become

$$\frac{d}{dt} I = -q_{iT} + q_{1T} + \rho_1 c T_1 \frac{dh}{dt}, \quad (23)$$

$$\frac{d}{dt}(H_1 \rho_1 c T_1) = -q_{1T} + q_{2T} - \rho_1 c T_1 \frac{dh}{dt} + \rho_2 c T_2 W, \quad (24)$$

$$\frac{d}{dt}(H_2 \rho_2 c T_2) = -q_{0T} - q_{2T} - \rho_2 c T_2 W, \quad (25)$$

where  $I$  is the net (negative) heat content of the ice sheet (per unit area). To calculate  $I$  accurately, one must take into account the fact that the specific heat of salt-ice ( $c_i$ )

depends strongly on the temperature. This occurs because the salt-ice is a mixture of pure ice, brine and (at  $T_i \lesssim -8^\circ\text{C}$ ) precipitated salt. When the temperature of salt-ice, which forms at the freezing point ( $T_f$ ), decreases below  $T_f$ , some new ice is formed from the brine in accordance with (6), where  $S$  now is the salinity of brine. Accurate estimates for  $c_i$  are given by (Schwerdtfeger 1963; Pounder 1965)

$$c_i = \lambda a S_i / T_i^2 - a S_i (c - c_0) / T_i + c_0 (1 - S_i / 1000), \quad (26)$$

where  $\lambda$  is the latent heat ( $\lambda = 79 \text{ cal g}^{-1}$ ) and  $c_0 \approx c/2$  is the specific heat of pure ice,  $c$  is the specific heat of water,  $S_i$  is measured in p.p.t. (‰) and  $a$  is defined in (6). Using (26), the net (negative) heat content ( $I$ ) of the ice sheet can be estimated as

$$I = c \rho_i T_f h - \lambda_i \rho_i h + \int_0^h \int_{T_f}^{T_i} \rho_i c_i dT_i dz, \quad (27)$$

where  $\lambda_i = \lambda(1 - S_i/S_1)$  is the latent heat of salt-ice and  $\rho_i \approx \text{const}$  ( $\approx 0.92 \text{ g cm}^{-3}$ ). Here the first term gives the heat content of salt water, which was initially at near the freezing point; the second term gives the latent heat of salt-ice formation near the freezing point and the last term gives the heat content of salt-ice which was cooled from the freezing temperature ( $T_f$ ) to the salt-ice temperature ( $T_i$ ) at a depth  $z$  in the ice sheet.

The full set of equations (16)–(27), together with proper parameterizations for such quantities as  $W$ ,  $q_{iS}$ ,  $q_{2S}$ ,  $q_{0T}$  and  $q_{iT}$  must be used in solving the problem. The resulting formulation, however, is too complicated for the analysis but can be simplified using a few standard assumptions while retaining a reasonable degree of accuracy.

(i) During freezing, the temperature of the upper layer is at near the freezing temperature ( $T_1 = T_f$ ), which is given by (6), and because the salinity  $S_1$  does not change significantly, let  $T_1 = T_f \approx \text{const}$ .

(ii) The density jump across the layers ( $\Delta\rho$ ) becomes important only when it is multiplied by some large coefficient, for example, when  $g\Delta\rho$  (where  $g$  is the gravitational acceleration) is used (see below). Thus, it can be assumed that  $\rho_1 \approx \rho_2 \approx \rho_i = \text{const}$ .

(iii) The salt transport ( $q_{2S}$ ) across the density interface, induced by the double-diffusive convection in the bottom layer, depends strongly on the heat transport ( $q_{2T}$ ) and on the density ratio  $R = \beta\Delta S/\alpha\Delta T$  ( $\beta$ ,  $\alpha$  are coefficients of salinity contraction and thermal expansion), and for  $R \geq 2$  the salt flux  $q_{2S}$  is parameterized by (Turner 1979)

$$q_{2S}/q_{2T} \approx 0.15\alpha/\beta. \quad (28)$$

In the experiment,  $R$  is large and  $\alpha/\beta$  is small because at low temperatures  $\alpha$  becomes very small. For example  $\alpha = 5.1 \times 10^{-5} (\text{°C})^{-1}$  at  $0^\circ\text{C}$  and  $\alpha = 10^{-5} (\text{°C})^{-1}$  at  $-2^\circ\text{C}$  for a salinity of 35‰ (Popov et al. 1979), and  $\beta [= 8 \times 10^{-4} (\text{‰})^{-1}]$  does not change with temperature significantly. Thus, it is possible to assume  $q_{2S} \approx 0$ .

(iv) The entrainment velocity ( $W$ ) induced by the salt convection in the upper layer strongly depends on the Richardson number ( $Ri$ ) at the interface,

$$Ri = g\Delta\rho l/u^2 \rho \quad (29)$$

( $\Delta\rho/\rho = \beta\Delta S - \alpha\Delta T \approx \beta\Delta S$  and  $l$ ,  $u$  are given in (9)) and  $W \approx 0$  at  $Ri \geq 35$  (Fernando 1989). In the present experiments typically  $Ri \geq 50$ , and the observations

show that during the experiments the interface practically does not move from its initial position (see figure 11, 12). Thus, it is possible to approximate  $W \approx 0$ .

Using the above simplifications, and using (5), (6), (10)–(16), the set of equations (17)–(27) can be reduced to

$$(d/dt)(h + H_1) = 0, \quad (30)$$

$$(d/dt)H_2 = 0, \quad (31)$$

$$H_1(dS_1/dt) = (S_1 - S_i)dh/dt, \quad (32)$$

$$(d/dt)S_i = 0, \quad (33)$$

$$(d/dt)S_2 = 0, \quad (34)$$

$$(d/dt)T_1 = 0, \quad (35)$$

$$\rho c H_2 (d/dt)T_2 = -q_{0T} - q_{1T}, \quad (36)$$

$$\begin{aligned} \rho \frac{d}{dt} h \left\{ -\lambda \left[ 1 + \frac{nT_f}{(T_f - T_0)} \ln \left( \frac{T_0}{T_f} \right) \right] - \frac{ncT_f}{2} \left[ \frac{T_0}{(T_f - T_0)} \ln \left( \frac{T_0}{T_f} \right) + 1 \right] + \frac{c}{4}(T_0 - T_f) \right\} \\ = K_i \frac{T_0 - T_f}{h} + q_{1T}, \end{aligned} \quad (37)$$

$$K_a \frac{T_0 - T_a}{\delta} = K_i \frac{(T_f - T_0)}{h}, \quad (38)$$

where (10) and  $n = S_i/S_1 \approx \text{const.}$  were used to calculate the integral in (27).

For the range of  $T_0$  used in the experiments, the two last terms on the left-hand side of (37) are small ( $\lesssim 2\%$ ) and can be neglected. Inserting  $T_0$  from (38) into (37), and solving the resulting equation with the condition  $h = 0$  at  $t = 0$ , one obtains for the non-dimensional thickness of the ice sheet

$$t^* = \int_0^{h^*} \frac{1 + h^*}{T_a^* - 1 - q_{1T}^*(1 + h^*)} \left\{ 1 - \frac{n}{(T_a^* - 1)} \ln \left[ \frac{1 + h^* T_a^*}{1 + h^*} \right] - \frac{n}{1 + h^* T_a^*} \right\} dh^*, \quad (39)$$

where, for brevity, the non-dimensional variables are denoted by stars; they are defined as

$$h^* = \frac{h}{\delta_1}, \quad \delta_1 = \delta \frac{K_i}{K_a}, \quad T_a^* = \frac{T_a}{T_f}, \quad q_{1T}^* = -\frac{\delta_1 q_{1T}}{K_i T_f}, \quad t^* = -\frac{K_i T_f t}{\delta_1^2 \rho \lambda}.$$

In these non-dimensional variables,

$$T_0^* = \frac{1 + h^* T_a^*}{1 + h^*}, \quad (40)$$

$$q_{aT}^* = \frac{T_a^* - 1}{1 + h^*}. \quad (41)$$

Solving (32) and (36), one obtains

$$\frac{\Delta S}{\Delta S_0} = 1 - \frac{(1 - S_i^*)h^*}{(S_2^* - 1)(H_0^* - h^*)}, \quad (42)$$

$$\frac{\Delta T}{\Delta T_0} = 1 - \frac{(\lambda/cT_f)q_{\Sigma}^* t^*}{H_2^*(T_2^{0*} - 1)}, \quad (43)$$

where

$$T_0^* = \frac{T_0}{T_f}, \quad q_{aT}^* = -\frac{\delta_1 q_{aT}}{K_1 T_f}, \quad S_i^* = \frac{S_i}{S_0}, \quad S_2^* = \frac{S_2}{S_0}, \quad H_0^* = \frac{H_0}{\delta_1}, \quad T_2^{0*} = \frac{T_2^0}{T_f}$$

and

$$S_0 = S_1, \quad H_0 = H_1, \quad T_2^0 = T_2 \quad \text{at } t = 0.$$

From (42), one obtains the estimate for  $h = h_0$ , when  $\Delta S = 0$ , as

$$h_0 = H_0 \left[ 1 - \frac{(S_0 - S_i)}{(S_2 - S_i)} \right], \quad (44)$$

which coincides with Zubov's estimate (1) for the maximum ice thickness, if the ice salinity is neglected ( $S_i = 0$ ). Note also that  $\Delta S = 0$  can be considered as the criterion for the initiation of overturning of the layers. When ice salinity is neglected and  $q_{1T} = 0$ , the estimate (39) for the non-dimensional thickness becomes

$$h^* + \frac{1}{2}(h^*)^2 = (T_a^* - 1)t^*, \quad (45)$$

and this equation has been widely used by many authors but with different empirical coefficients (see e.g. Anderson 1961; Maykut 1986; Doronin 1970). The present formulation provides a theoretical foundation for such empirical formulations.

From (39) it is clear that, for young sea ice, the effect of relatively large ice salinity (which is incorporated into (39) via  $n = S_i/S_1$ ) is to increase the rate of ice formation. On the other hand, the presence of warm water under the cold upper layer ( $q_{1T}^* > 0$ ) impedes ice formation.

The measured and calculated (using (39)) ice thickness ( $h^*$ ) as a function of time ( $t^*$ ) are shown in non-dimensional form in figure 16 for two experiments with homogeneous fluid and one experiment with two-layer stratification. In calculations for the homogeneous fluid,  $q_{1T}^* = -q_{0T}^* = -1.3$ , as estimated using (5), was used for  $T_a = -12^\circ\text{C}$ , and  $q_{0T}^* = 2.35$  was used for  $T_a = -19^\circ\text{C}$ . For the stratified case ( $T_a = -19^\circ\text{C}$ )  $q_{1T}^* = 2.3$ , as estimated using (14) and (15), was used until  $h^* \leq h_0^*$  and then  $q_{1T}^* = -2.35$  was used. The measured and calculated values, using (40), of the non-dimensional ice surface temperature ( $T_0^*$ ) for these experiments are compared in figure 17, while the measured and calculated values, using (42) and (43), of  $\Delta S/\Delta S_0$  and  $\Delta T/\Delta T_0$  for the experiment with a stratified fluid are given in figure 14.

As can be seen from these comparisons, the model, in spite of significant simplifications, describes most of the experimental observations satisfactorily. Deviation of the model estimate of  $\Delta S/\Delta S_0$  from the experimental data (figure 14) may be a result of underestimation of the salt flux ( $q_{is}$ ) rejected from the ice sheet. The simplified model considered above gives  $q_{is} \propto dh/dt$  for this flux, while the results of direct measurements (for example, see figure 12 in Wakatsuchi & Ono 1983) show that  $q_{is} \propto (dh/dt)^{1/2}$ . At present the physical reasons for this disparity are not clear, and more detailed studies are required to address this issue.

## 5. Conclusions

In this paper, processes associated with ice formation in a two-layer fluid system subjected to surface cooling were described. The fluid system consisted of a layer of cold, relatively less salty water placed above a warmer, salty water layer so that the overall system is statically stable. Some experiments were also carried out with homogeneous salty water. It was found that the rate of ice formation in the

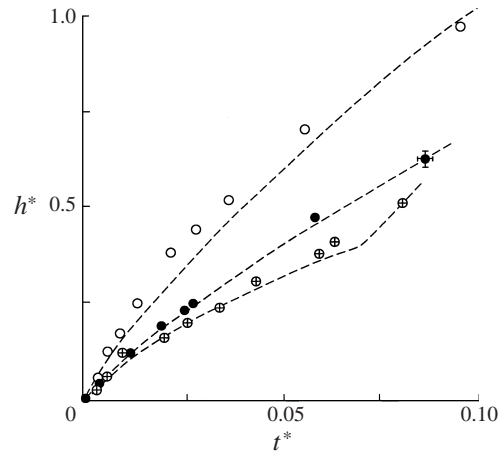


FIGURE 16. Measured (points) and calculated (using (39)) (dashed lines) values of the non-dimensional ice thickness ( $h^*$ ) as a function of non-dimensional time ( $t^*$ ) for two experiments carried out with a homogenous fluid at  $T_a = -12^\circ\text{C}$  ( $\bullet$ ),  $-19^\circ\text{C}$  ( $\circ$ ) and an experiment carried out with a stratified fluid at  $T_a = -19^\circ\text{C}$ . ( $\oplus$ ).

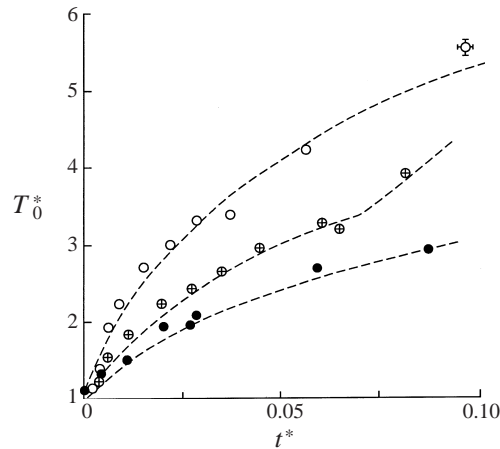


FIGURE 17. Measured (points) and calculated (using (40)) (dashed lines) values of the non-dimensional ice-surface temperature ( $T_0^*$ ) as a function of the non-dimensional time ( $t^*$ ) for the experiments described in figure 16.

stratified case can be significantly lower than in the case of a homogenous salt water layer having identical properties to that of the upper layer of the two-fluid system. In the two-layer case, the salinity jump between the layers decreases with the time and eventually the fluid system becomes unstable, leading to overturning and mixing. Thereafter, the temperature of water under the ice sheet increases above the freezing point and some melting of ice is possible. The relatively small depth (or low heat content) of the bottom layer used in the present experiments, however, did not permit significant melting of ice during the overturning of layers; instead, immediately following the overturning, the ice sheet in the experiments continued to grow at an increased rate. We expect ice melting due to overturning to be present in some geophysical cases, especially in southern oceans, where the bottom layer is deep and contains sufficient heat to provide latent heat necessary for ice melting.

Low ice thicknesses observed in southern oceans, in part, may be attributable to such phenomena.

A simplified theoretical model was proposed to explain the experimental observations. Although this model can describe most of the flow characteristics with a reasonable accuracy, it underestimates the magnitude of the salt flux rejected from the growing ice sheet. Also, it relies on several empirical parameterizations, for example, for the heat transport between warm and cold layers. The relative success of the model proposed herein attests to the general suitability of the parameterizations employed in its development, but much improvement can be made to these parameterizations to enhance their versatility. Further studies are necessary to address the observed disparities and to develop improved parameterizations for ice-related processes in polar oceans.

This work was primarily supported by a grant from the Office of Naval Research (High-Latitude Dynamic Program). Stratified and rotating turbulent flow research at Arizona State University is also supported by the Office of Naval Research (Physical Oceanography Program), the National Science Foundation (Fluid Mechanics Program) and the Army Research Office (Engineering and Environmental Sciences Directorate).

#### REFERENCES

- AGAARD, K., COACHMAN, L. K. & CARMACK, E. C. 1981 On the halocline of the Arctic ocean. *Deep-Sea Res.* **28**, 529–545.
- ACKLEY, S. F., CLARKE, D. B. & SMITH, S. J. 1982 Weddell polynya expedition preliminary data report: Physical, chemical and biological properties of ice cores. *Tech. Note US Army Cold Water Regions Research and Engineering Lab., Hanover, NH.*
- ANDERSON, D. L. 1961 Growth rate of sea ice. *J. Glaciol.* **3**, 1170–1172.
- ATKINSON, J. F. & WAKE, A. 1988 Double-diffusive convection under sea ice. *ASCE J. Cold Regions Engng* **2**, 89–95.
- COACHMAN, L. K. & AGAARD, K. 1974 Physical oceanography of arctic and subarctic seas. In *Marine Geology and Oceanography of the Arctic Seas*, pp. 1–72. Springer.
- DORONIN, YU. P. 1970 *Thermal Interaction of the Atmosphere and the Hydrosphere in the Arctic*. Israel Program for Scientific Translation, Jerusalem.
- E, X. & HOPFINGER, E. J. 1986 On mixing across an interface in stably stratified fluid. *J. Fluid Mech.* **166**, 227–244.
- ETTEMA, R., KARIM, M. F. & KENNEDY, J. F. 1984 Laboratory experiments on frazil ice growth in supercooled water. *Cold Region Sci. Technol.* **10**, 43–58.
- FARHADIEH, R. & TANKIN, R. S. 1972 Interferometric study of freezing of sea water. *J. Geophys. Res.* **77**, 1647–1657.
- FERNANDO, H. J. S. 1989 Buoyancy transfer across a diffusive interface. *J. Fluid Mech.* **209**, 1–34.
- FOSTER, T. 1969 Experiments on haline convection induced by the freezing of sea water. *J. Geophys. Res.* **74**, 6967–6974.
- FOSTER, T. D. & CARMACK, E. C. 1976 Temperature and salinity structure in the Weddell sea. *J. Phys. Oceanogr.* **6**, 36–44.
- GORDON, A. L. & HUBER, B. A. 1990 Southern ocean winter mixed layer. *J. Geophys. Res.* **95**, 11655–11672.
- HUBER, B. A., MELE, P. & GORDON, A. L. 1989 Report of the Winter Weddell Sea Project, ANT V/II, Hydrographic Data, L-DGO-89-1, Lamont-Doherty Geological Observatory, Palisades, NY.
- HUPPERT, H. E. 1971 On the stability of a series of double-diffusive layers. *Deep-Sea Res.* **18**, 1005–1021.
- KATSAROS, K. B. & LIU, W. T. 1974 Supercooling at a free salt water surface in the laboratory. *J. Phys. Oceanogr.* **4**, 654–658.

- KIT, E., STRANG, E. & FERNANDO, H. J. S. 1997 Measurement of turbulence near shear-free density interfaces. *J. Fluid Mech.* **334**, 293–314.
- LAKE, R. A. & LEWIS, E. L. 1970 Salt rejection by sea ice during growth. *J. Geophys. Res.* **75**, 583–597.
- LEWIS, E. L. & WEEKS W. F. 1971 Sea ice. Some polar contrasts. In *Symp. on Antarctic Ice and Water Masses* (ed. G. Deacon), pp. 28–38. Scott Polar Research Institute, University of Cambridge, England.
- LIDE, D. R. (Ed.) 1993 *CRC Handbook of Chemistry and Physics*. CRC Press.
- LINDEN, P. F. & SHIRTCLIFFE, T. G. L. 1978 The diffusive interface in double-diffusive convection. *J. Fluid Mech.* **87**, 471–432.
- MARTIN, S. 1981 Frazil ice in rivers and oceans. *Ann. Rev. Fluid Mech.* **13**, 379–397.
- MARTINSON, D. G. 1991 Open ocean convection in southern ocean. In *Deep Convection and Deep Water Formation in Oceans* (ed. P. C. Chu & J. C. Gascard), pp. 37–52. Elsevier.
- MAYKUT, G. A. 1986 The surface heat and mass balance. In *The Geophysics of Sea Ice* (ed. N. Untersteiner), pp. 395–461. Plenum.
- NAKAWO, M. & SINHA, N. K. 1981 Growth rate and salinity profile of first-year sea ice in the high arctic. *J. Glaciol.* **27**, 315–330.
- NIEDRAUER, T. M. & MARTIN, S. 1979 An experimental study of brine drainage and convection in young sea ice. *J. Geophys. Res.* **84**, 1176–1185.
- OMSTED, A. 1985 On supercooling and ice formation in turbulent sea-water. *J. Glaciol.* **31**, 263–270.
- POPOV, N. I., FEDOROV, K. N. & ORLOV, V. M. 1979 *Sea Water*. Nauka, Moscow (in Russian).
- POUNDER, E. R. 1965 *The Physics of Ice*. Pergamon.
- SCHWERDTFEGER, P. 1963 The thermal properties of sea ice. *J. Glaciol.* **4**, 789–807.
- TURNER, J. S. 1979 *Buoyancy Effects in Fluids*. Cambridge University Press.
- UNTERSTEINER, N. 1968 Natural desalinization and equilibrium salinity profile of perennial sea ice. *J. Geophys. Res.* **73**, 1251–1257.
- VOROPAYEV, S. I., FERNANDO, H. J. S. & MITCHELL, L. A. 1995 On the rate of frazil ice formation in polar regions in the presence of turbulence. *J. Phys. Oceanogr.* **25**, 1441–1450.
- WAKATSUCHI, M. & ONO, N. 1983 Measurements of salinity and volume brine excluded from growing sea ice. *J. Geophys. Res.* **88**, 2943–2951.
- WALIN, G. 1993 On the formation of ice on deep weakly stratified water. *Tellus* **45 A**, 143–157.
- WEEKS, W. F. & ACKLEY, S. F. 1986 The growth, structure, and properties of sea ice. In *The Geophysics of Sea Ice* (ed. N. Untersteiner), pp. 9–165. Plenum.
- WELANDER, P. & BAUER, J. 1977 On a differentially heated saltwater-ice system. *Tellus*. **29**, 462–469.
- ZUBOV, N. N. 1938 On the maximum thickness of perennial sea ice. *Meteorologiya i Gidrologiya* **4**, 123–131 (in Russian).
- ZUBOV, N. N. 1963 *Arctic Ice*. US Naval Oceanographic Office and American Meteorological Society. (First published in Russian by Glavsevmorput in 1945.)